Materials Science in Semiconductor Processing 33 (2015) 127–135

Contents lists available at ScienceDirect

Materials Science in Semiconductor Processing

journal homepage: www.elsevier.com/locate/mssp

Structural, mechanical and electronic properties of sodium based fluoroperovskites $NaXF_3$ (X=Mg, Zn) from first-principle calculations

R. Arar [a], T. Ouahrani [b], D. Varshney [c,*], R. Khenata [d], G. Murtaza [e], D. Rached [f], A. Bouhemadou [g], Y. Al-Douri [h,i], S. Bin Omran [j], A.H. Reshak [k]

[a] Department of Physics, University Amar Telidji of Laghouat, Laghouat 03000, Algeria
[b] Laboratoire de Physique Théorique, Université de Tlemcen, B.P.230, 13000 Tlemcen, Algeria
[c] Materials Science Laboratory, School of Physics, Vigyan Bhavan, Devi Ahilya University, Khandwa Road Campus, Indore 452001, India
[d] Laboratoire de Physique Quantique et de Modélisation Mathématique, Université de Mascara, Mascara 29000, Algeria
[e] Materials Modeling Laboratory, Department of Physics, Islamia College University, Peshawar, Pakistan
[f] Laboratoire des Matériaux Magnétiques, Université de Sidi Bel Abbés, Sidi Bel Abbés 22000, Alegria
[g] Laboratory for Developing New Materials and their Characterization, Department of Physics, Faculty of Science, University of Setif, 19000 Setif, Algeria
[h] Institute of Nano Electronic Engineering, University Malaysia Perlis, 01000 Kangar, Perlis, Malaysia
[i] Physics Department, Faculty of Science, University of Sidi-Bel-Abbes, Sidi Bel Abbés 22000, Algeria
[j] Department of Physics and Astronomy, College of Science, King Saud University, P.O. Box 2455, Riyadh 11451, Saudi Arabia
[k] School of Complex Systems, FFPW, CENAKVA, University of South Bohemia in CB, Nove Hrady 37333, Czech Republic

ARTICLE INFO

Keywords:
DFT, Perovskites
Elastic constants
Electronic properties
Thermal properties

ABSTRACT

The structural stability, mechanical, electronic and thermodynamic properties of the cubic sodium based fluoro-perovskite $NaXF_3$ (X=Mg, Zn) have been studied using density functional theory (DFT). The generalized gradient approximation of Perdew–Burke and Ernzerhof (GGA-PBE) is used for modeling exchange-correlation effects. In addition, the alternative form of the GGA proposed by Engel and Vosko (GGA-EV) is also used to improve the electronic band structure calculations. The results show that both compounds are stable in the cubic *Pm3m* structure. From Poisson's ratio, it is inferred that cubic anti-perovskite $NaXF_3$ are ductile in nature and that bonding is predominantly of ionic in nature. The electronic band structure calculations and bonding properties show that anti-perovskites have an indirect energy band gap (M–Γ) with a dominated ionic character. The thermal effects on thermal expansion coefficient, Debye temperature and Grüneisen parameter were predicted using the quasi-harmonic Debye model, in which the lattice vibrations are taken into account. The calculations are found to be in good agreement with other results.

1. Introduction

The fluoroperovskites crystals are constantly a subject of thorough and intensive investigations. The leitmotiv of this deep interest is due to their relatively simple crystal structure that displays many diverse electric, magnetic, piezoelectric, optical, catalytic and magnetoresistive properties. In

* Corresponding author. Tel./fax: +91 7312467028.
E-mail address: vdinesh33@rediffmail.com (D. Varshney).

http://dx.doi.org/10.1016/j.mssp.2015.01.040
1369-8001/

the recent past, crystals with ABF_3 formula have been a subject of immense interest due to high temperature proton conductors with the possibility of applications in fuel cells or hydrogen sensors [1–4] and also due to enhanced technological demands on optical lithography in semiconductors. These are possibly used as lens materials because they do not have birefringence, which makes design of lenses difficult [5–8]. Also, the possible problems in using optical materials for the UV and VUV regions are their limited transmission and the difficulty of material processing and polishing due to cleavage or the hydroscopic nature of the materials. The centrosymmetric $NaMgF_3$ and $NaZnF_3$, which crystallize in cubic perovskite and orthorhombic postperovskite [9], do not have these problems, and so, will be appropriate optical materials for the UV and VUV regions [10,11].

The determination of the geometry and stability of an arbitrary material represents a necessary starting point for the complete characterization of the material properties. Understanding the high pressure behavior of solids requires rationalizing how and why matter compresses under external stresses. Though, it is clear that the macroscopic compressibility of a crystal is ultimately determined by its chemical bonds and its valence electrons, so it is proved that a systematic and quantitative correlation in quantum chemical terms exist between electronic, thermal and optical calculations [12]. State of the art investigations and appropriate benchmark of density functional theory (DFT) computation are published elsewhere [13].

Both $NaMgF_3$ and $NaZnF_3$ can undergo phase transitions at high pressure, as the family of the perovskites, some of them might prefer to undergo a $CaIrO_3$ type postperovskite *Pbnm* or *Pnma* type transition to another ABX_3 polymorph before dissociating. A *Cmcm* phase might also be observed metastable at low temperatures if the energy barrier for dissociation is large, or its products (AX and BX_2) have a limited stability range [14]. Recently, two potential candidate structures for the $NaMgF_3$ compound at very high pressure >50 GaP, are noticed with symmetries *Pmcn* and *P63/mmc* [14]. However, the phenomenological theoretically and experimentally study of Zhao et al. [15] does not exclude the possibility of existence of the *Pm3m* cubic phase. Using X-ray diffraction and Bragg's relationship, the authors provide a critical analysis related to the centrosymmetrically distortion of these perovskites, they have demonstrated two decoupled mechanisms for thermal expansion and compression, i.e., thermal expansion is mostly accommodated by octahedral tilting and compression is dominated by changes in the octahedral bond lengths. Another measure based on the idea cited above, Chen et al. [16] have explained that an orthorhombic (*Pbnm*) to cubic (*Pm3m*) transition is observed when the temperature is increased from 900 to 1000 °C.

In the present work, we have chosen the cubic phase of the two fluoroperovskites $NaMgF_3$ and $NaZnF_3$ as the main subject with an aim of getting consistent and unified comparative density functional theory (DFT)-based description of their properties under pressure. Our motivation is to present here research to enlarge extension driven by the fact that despite a rather simple structure of these materials, surprisingly not much has been reported so far on their electronic, elastic properties. Furthermore, the theoretical predictions of the compounds are not treated with recent developed potentials like modified Becke–Johnson potential. Therefore, this work is very important concerning the basic treatment of the fundamental properties. This work will also cover the lack of data on these important compounds and provide reference data for further experimental or theoretical calculations.

2. Computational details

All calculations presented here were performed using the full-potential linearized augmented plane wave (FP-LAPW) method [18] based on density functional theory DFT [19,20] and implemented in wien2K package code [21]. The electronic exchange-correlation potential was calculated by using the general gradient approximation (GGA) within the Perdew–Burke–Ernzerhof (PBE) scheme [22]. We have also used the Engel–Vosko GGA [23] scheme and the modified Becke–Johnson scheme [24] to determine the band structure. In the interstitial region, a plane wave expansion with $R_{MT}\times K_{\max}=8$ and 8.5 where R_{MT} is the minimum radius of the muffin-tin spheres and $K_{\max}$ gives the magnitude of the largest K vector in the plane wave basis. The potential and the charge density were Fourier expanded up to $G_{\max}=12$ (a.u.)$^{-1}$. The valence wave functions inside the atomic muffin-tin-spheres were expanded to $l=10$ in the irreducible wedge of the first Brillouin zone (IBZ) that has been explored within the tetrahedron method and the size of the mesh has been set to $17\times17\times17$ points [25]. The self-consistency was achieved since the total energy difference between successive iterations was less than 10^{-5} Ryd per formula unit.

3. Results and discussion

3.1. Ground states and elastic properties

The stability of the crystal should be addressed with respect to solid-state reactions produces compounds of different AMX_3 stoichiometry with different crystalline structure. The present studies of polymorph has made for pressures lower than 50 GPa. Table 1 gives the optimized lattice constants for all the polymorph of the considered crystals, as appeared after performing geometry optimization with the above-given computational settings. Inspection of data from this table shows that all the calculated parameters are slightly overestimated in comparison with the available data. Such a trend is in line with the calculated lattice constants for $NaMgF_3$ and $NaZnF_3$ as given earlier [26]. The non cubic phases have a simple orthorhombic unit cell with 20 atoms (please see Table 1). Our calculations confirm that the $Pm\bar{3}m$ cubic phase is the most stable (please see Fig. 1), in good agreement with the experimental prediction [9,27].

Using, PBE-GGA calculations, the lattice constant of cubic $NaMgF_3$ and $NaZnF_3$ are sketched in Fig. 2 and predicted as 3.964 Å and 4.065 Å respectively, which are in good agreement with the experimental values (3.84 Å for $NaMgF_3$ and 3.88 Å for $NaZnF_3$) [18]. The elastic constants and their pressure dependence for these compounds are also computed using tetrahedral and rhombohedral distortions for the cubic structure. The system is fully relaxed after each distortion in order to reach the equilibrium state with

Table 1
Lattice constants and Wyckoff coordination of $NaMgF_3$ and $NaZnF_3$ in the *Cmcm*, *Pnma* and *Pm3m* phases.

Cmcm	**$NaMgF_3$**			**$NaZnF_3$**		
(a, b, c)	3.07 2.773 [14]	10.39 8.682 [14]	7.48 6.876 [14]	3.13	10.46	7.62
	x	***y***	***z***	***x***	***y***	***z***
Na (4c)	0.0	0.2610	3/4	0.0	0.2580	¾
Mg/Zn (4a)	0.0	0.0	0.0	0.0	0.0	0.0
F1 (4c)	0.0	0.9283	3/4	0.0	0.9200	¾
F2 (8f)	0.0	0.3762	0.0560	0.0	0.3737	0.0586
Pnma	**$NaMgF_3$**			**$NaZnF_3$**		
(a, b, c)	5.59	7.79	5.44	5.57	8.00	5.55
	x	***y***	***z***	***x***	***y***	***z***
Na (4c)	0.5459	¼	0.4876	0.5536	1/4	0.4862
Mg/Zn (4a)	0.0	0.0	1/2	0.0	0.0	½
F1 (4c)	0.0312	¾	0.4053	0.0427	3/4	0.3924
F2 (8f)	0.7926	0.4509	0.2056	0.6997	0.9442	0.6978
$Pm\bar{3}m$	3.964, 3.84 [17]			4.065, 3.88 [17]		

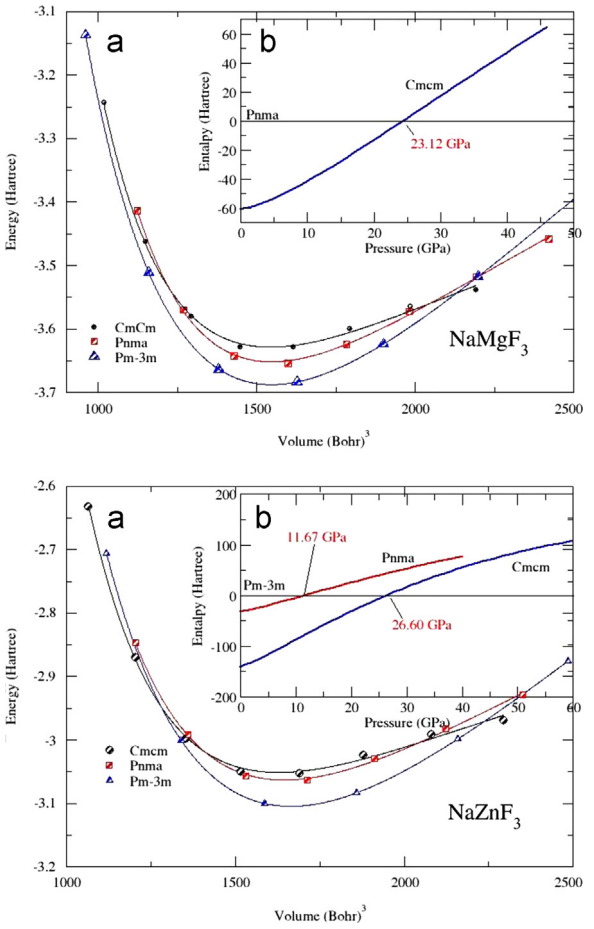

Fig. 1. The calculated total energies in *CmCm*, *Pnma* and *Pm3m* structures of $NaMgF_3$ (a) and $NaZnF_3$ (b).

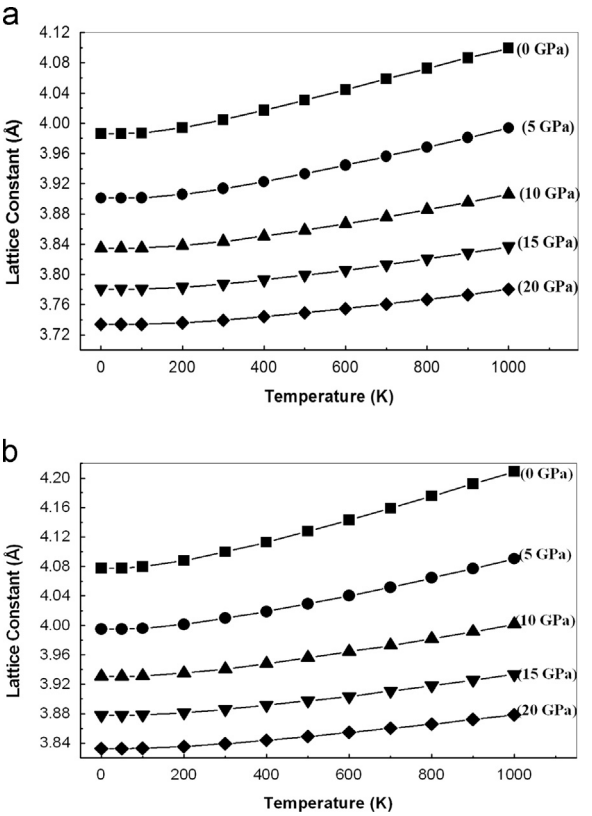

Fig. 2. Lattice constant versus pressure and temperature of $NaMgF_3$ (a) and $NaZnF_3$ (b).

approximately zero forces on the atoms. The elastic properties are described by 36 elastic stiffness constants for anisotropic crystalline solid.

For the cubic crystal, due to its higher symmetry, the number of elastic stiffness constant reduces into 3 such as C_{11} (relates the longitudinal or compression stress and strain along ⟨100⟩ directions), C_{44} (relates the transverse or shear stress and strain in the same directions) and C_{12} (relates the longitudinal stress in one direction to the strain in another direction). Our results regarding C_{11}, C_{12}, C_{44} and bulk modulus B at equilibrium cubic phase

Table 2
Calculated elastic constants C_{ij} (in GPa), Bulk modulus B (in GPa), Shear modulus G (in GPa), Young's modulus and Poisson's ratios σ, for cubic $NaMgF_3$ and $NaZnF_3$ compounds.

	C11 (GPa)	C_{12} (GPa)	C_{44} (GPa)	B (GPa)	G (GPa)	B/G	E (GPa)	σ
$NaMgF_3$	136.9082	31.8473	51.0104	66.8676	51.613	1.296	123.1532	0.193
$NaZnF_3$	135.0395	39.6591	41.9587	71.4526	44.164	1.62	109.8589	0.243

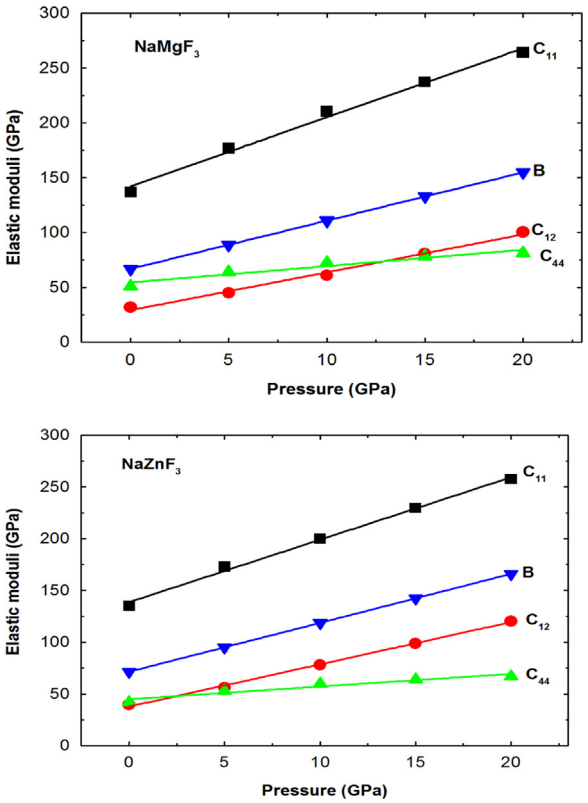

Fig. 3. Elastic moduli versus pressure of $NaMgF_3$ and $NaZnF_3$.

are listed in Table 2. We comment that the unidirectional elastic constant C_{11}, which is related to the unidirectional compression along the principal crystallographic directions, is about 77% higher than C_{44} for $NaMgF_3$ and 71% for $NaMgF_3$, indicating that these compounds present a weaker resistance to the pure shear deformation compared to the resistance of the unidirectional compression. According to our knowledge, the experimental and theoretical calculations are not available in the literature.

The variation of the elastic constants as a function of pressure is displayed in Fig. 3. We observe that all elastic constants show a linear increasing as the pressure increases. We have found, after some initial surprise, that the behavior of the lattice constant is rather quadratic under the effect of pressure. This behavior reflects that the dependence of pressure is more complicated trends and can be subjected to more studies to be well applied [13,26]. For cubic crystals, the mechanical stability requires the elastic constants satisfying the well-known Born stability criteria:

$$\begin{aligned} &C_{11} > |C_{12}| \\ &(C_{11}+2C_{12}) > 0 \\ &C_{44} > 0 \end{aligned} \tag{1}$$

From the calculated C_{ij} as listed in Table 2, the above criteria are satisfied indicating that the perovskites $NaMgF_3$ and $NaZnF_3$ are mechanically stable. A problem arises when single crystal samples cannot be obtained, for that it is not possible to measure the individual elastic constants C_{ij}. Instead, the isotropic bulk modulus B and shear modulus G are determined. These quantities cannot be calculated directly from the C_{ij}, but we can use the computed values to place bounds on the isotropic moduli. Reuss [28] determines lower bounds for all lattices, while Voigt [29] suggests upper bounds [30]. For the specific case of cubic lattices, Hashin and Shtrikman [31] have found stricter bounds. The isotropic bulk modulus for the cubic system is given by

$$B_{V,R} = 1/3(C_{11}+2C_{12}) \tag{2}$$

The Reuss and Voigt limits for the shear modulus are

$$G_R = \frac{5C_{44}(C_{11}-C_{12})}{[4C_{44}+3(C_{11}-C_{12})]} \tag{3}$$

$$G_V = \frac{C_{11}-C_{12}+3C_{44}}{5} \tag{4}$$

The shear modulus G is given by

$$G = \frac{G_V+G_R}{2} \tag{5}$$

Another quantity associated with the volume during uniaxial deformation and the stability of the material against shear is Poisson's ratio as given by

$$\sigma = (3B-E)/6B \tag{6}$$

where E is the Young modulus. It takes the value in between -1 and 0.5. The lowest value of Poisson's ratio indicates a large volume deformation, when $\sigma=0.5$ there is no volume changes. Poisson's ratio also provides more information for dealing with the characteristic of the bonding forces. For covalent materials it is small ($\sigma \approx 0.1$), whereas for ionic materials a typical value of $\sigma=0.25$ [32]. In the present case, σ varies from 0.193 ($NaMgF_3$) to 0.243 ($NaZnF_3$), i.e. according to this index, a higher ionic contribution in intra-atomic bonding for perovskites $NaMgF_3$ and $NaZnF_3$ should be assumed.

Mechanical properties such as brittleness, ductility and hardness of the materials can be understood using elastic constants. Cauchy's pressure is given by C_{12}–C_{44} will serve as an indication of ductility. Cauchy pressure describes the angular characteristics of atomic bonds in metals and

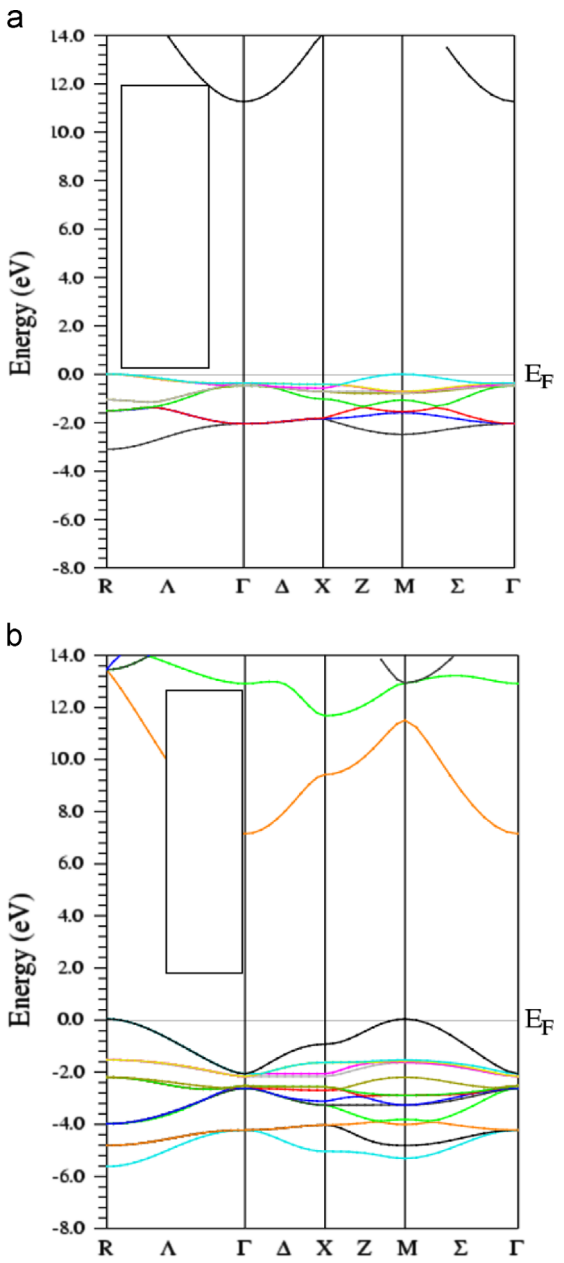

Fig. 4. The mBJ-GGA band structures of $NaMgF_3$ (a) and $NaZnF_3$ (b).

compounds. The positive Cauchy pressure reveals the metallic nature and the negative pressure suggests an angular or directional bonding. If the pressure is positive (negative), the material is expected to be ductile (brittle). Herein, the value of Cauchy's pressure is found to be equal to −19.17 GPa for $NaMgF_3$ and −2.3 GPa for $NaZnF_3$, which clearly highlights the brittle nature of these compounds.

The ductility/brittleness materials are also interpreted by (B/G) ratio. According to Pugh's [33], the high (low) B/G ratio is associated with the ductile (brittle) nature of the materials. The critical number that separates the ductile and brittle, was found to be 1.75. As listed in Table 2, for both compounds the B/G ratio is smaller than the critical

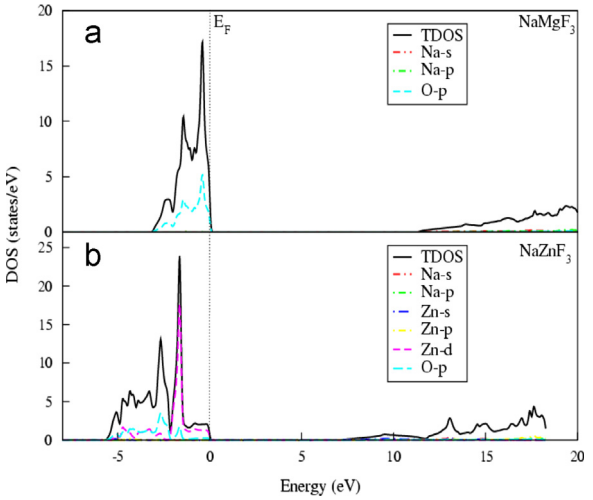

Fig. 5. Density of states of $NaMgF_3$ (a) and $NaZnF_3$ (b).

value, which also classified as brittle materials. We may also refer to Frantsevich et al. [34] who distinguished the ductility and brittleness of materials in terms of Poisson's ratio (σ). According to the Frantsevich rule, the critical value of material is 0.26. For brittle materials, Poisson's ratio is less than 0.26, otherwise the material behaves in a ductile manner, as recently demonstrated in a study of brittle versus ductile transition in some perovskite compounds from first-principles calculations [35,36]. Here the calculated Poisson's values are both smaller than 0.26, meaning that both $NaMgF_3$ and $NaZnF_3$ compounds are brittle in nature.

3.2. Electronic and bonding properties

The prediction of band gap energies of solids regards a major concern in simulation of solid state. Recently, Mori-Sánchez et al. [37] have associated the error in the band gap prediction of different functionals with their behavior upon fractional charges, that is, localization. Within the frontier orbital approach the hardness of solids is half its band gap [38]. The calculated energy band structures along the high symmetry directions in the Brillouin zone at zero pressure within the mBJ approximation are shown in Fig. 4. The valence band maximum (VBM) occurs at the M point of the Brillouin zone, whereas, the conduction band minimum (CBM) at the Γ point indicates an indirect band gap M–Γ. The calculated indirect gap is 5.99 eV ($NaMgF_3$), 3.35 eV ($NaZnF_3$) using GGA and 6.74 eV ($NaMgF_3$), 4.11 eV ($NaZnF_3$) using EV-GGA. Further mBJ potential is also applied to improve the bandgaps. The calculated indirect bandgap is 10.6 eV of $NaMgF_3$, 6.60 eV of $NaZnF_3$. It is well known that GGA and EV-GGA usually underestimate the gap of semiconductors and mBJ yields better value of energy gap. This value indicates insulator behavior. Density of States (DOS) of the compounds are also calculated and plotted in Fig. 5. For $NaMgF_3$, valence band is mainly composed of the O-2p states while the conduction band has mixed states of Na and O. While, For $NaMgF_3$, the valence band is composed of

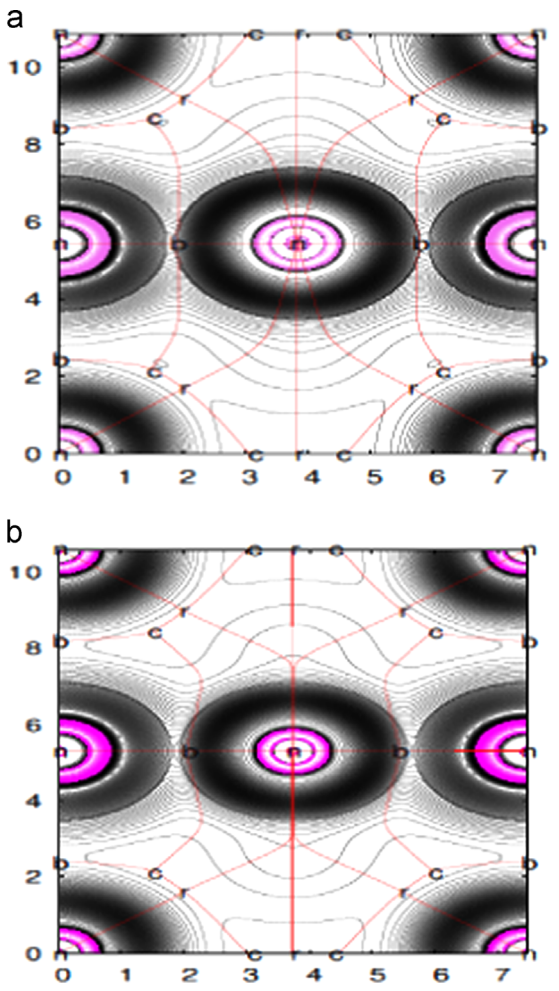

Fig. 6. Contour plot of the Laplacian of the electron density in a plane ([111]) containing the three non-equivalent atoms of $NaMgF_3$ (a) and $NaZnF_3$ (b). This plane contains all the CPs (*n*, *b*, *r* and *c*) of the structure: the three nuclei, the Na–F and Mg/Zn–F bond Cp's, a single ring Cp's, and two deferent cage Cp's. Red lines correspond to the atomic basins subdivision in 2D. (For interpretation of the references to color in this figure legend, the reader is referred to the web version of this article.)

mixed O-2p and Zn-3d states. The conduction band contains mixed states of Na, Zn and O.

As a numerical analysis the method based on the theory of atoms in molecules (AIM) of Bader [40] has proved its effectiveness. From the advent of visual AIM analysis given in Fig. 6, it was recognized that the ionic compounds are identified by electrostatic interaction between ions, where it is shown a lack of bonding basins and the sphericity of the ions. The enormous concentration of critical points hampered the complete topological characterization of these solids. Using (AIM) formalism as an alternative procedure for more explicit information on the bonding properties when considering the whole unit cell in crystals [40]. The electron density (ρ) is the central property of AIM. Via the topology of the electron density the concept of atoms and bonds can be introduced. The critical points (CP) of ρ, i.e., mark special positions in space. The critical points (CP), solutions to the equation $\vec{\nabla}\rho.\vec{n}=0$, are classified according to the Hessian or curvature matrix into: maxima or nuclear CP's (NCP or *n*), first order saddle or bond CP's (BCP or *b*), second order saddle or ring CP's (RCP or *r*) and minima or cage CP's (CCP or *c*). The number of CP's is regulated by topological invariants. In case of solids Morse's relationships ensures that $n-b+r-c=0$, $n, c\geq 1, b, r\geq 3$.

Using the critical points distribution shown in the plot of the {111} plane of the charge density (Fig. 6), and according to the structure satisfying Euler's relationship (faces − edges + vertices = 2), we can construct a polyhedra which contains all atomic attraction basins (see the red lines in Fig. 6). By means of the CRITIC [39] code, the atomic properties (P) are calculated by integrating their associated property densities ($p(r)$) inside the basins (Ω): $P_\Omega=\int_\Omega p(r)dr$, the scalar fields for atomic volumes ($p=1$, $P=V$) and charges ($p=\rho$, $P=N$) are readily available. The ions in $NaXF_3$ (X=Mg, Zn) crystals having according to the three dimensional plot in Fig. 6, an *R*9 topological scheme [42], can provide required information on the character of the bonding that using semi-empirical relations proposed by Mori-Sánchez et al. [41]; ionicity index is defined as an average for all the basins of the ratio between the local topological charge and the nominal oxidation state, $c=(1/N)\Sigma_{\Omega=1}^{N}(Q(\Omega)/\mathrm{OS}(\Omega))$ and charge-transfer index of the atom in crystal $\mathcal{CT}(\Omega)=1-(\mathrm{OS}(\Omega)-Q(\Omega))/\mathrm{OS}(\Omega)$.

These entire indexes are gathered in Table 3 according to Luaña et al. [42]. Here, $Q(\Omega)$ and OS (Ω), are the topological charge [43] and the nominal oxidation states, respectively. These perovskites behave clearly as ionic compounds, as indicated by the topological charges (see Table 3). The charge of the sodium ions is very close to the nominal +1 value, the Fluorine have an average charge $Q(\mathrm{X})=-0.8$ to -0.9, and the alkaline earth ions are $Q(\mathrm{Mg})=1.76$ and $Q(\mathrm{Zn})=1.44$ (electron). These investigated compounds according to Fig. 7 correspond to the dominant *R*9 family [44], where the magnesium basin is topologically equivalent to a cube. The result to calculate the index c is giving the degree of ionicity, predicted that our materials are dominated by nearby $>50\%$ by ionic global character. The charge transferred $\mathcal{CT}$ between atoms is considerable. However, it is clear there is a dominance of the ionic over the covalent character.

The topological analysis is particularly well suited to provide information on the nature of the chemical bond in crystals because the graphical representation of appropriate scalar fields on the surfaces of the basins gives illuminating images of the bonding situation. Thus, depicting directly the electron density, we can observe the zones of accumulation and depletion of charge reveal the presence of bond CPs. In Fig. 7, we show from the 2D electron density plot, the accumulation of density along the F–Zn bond is larger than those along the F–Na and F–Mg bonds.

According to Bader's formulation [45], every bond critical point (BCP) can be described by its position, electron density at this point, Hessian matrix eigenvalues $\lambda1$, $\lambda2$, $\lambda3$ and Laplacian $\nabla^2\rho(r)$. Negative values of the Laplacian ($\nabla^2\rho(r)<0$) are characteristic of covalent bonding (charge is concentrated between bonded atoms), while charge depletion in bond region associated with positive value of Laplacian ($V^2\rho(r)>0$) is characteristic of ionic bonding. Almost Laplacian values in the entitled compounds are positive, indicating charge depletion in the bonding region and very small electron

Table 3
AIM atomic properties of $NaXF_3$ (X=Mg, Zn) correspond to the multiplicity in the conventional unit cell, the integrated charge $\mathcal{Q}$, the degree of ionicity c and the charge transfer $\mathcal{CT}$ beside the electron density Laplacian $\nabla^2\rho(r)$ and the density of the BCP ρ_b^{max} point.

Atom	Wyck.	$\mathcal{Q}$ (electron)	CT	c		
$NaMgF_3$				59.47%		
Na	1a	+9.1978502391E-01	0.9599			
Mg	1b	+1.7565966449E+00	0.8783			
F	3c	−8.9171939090E-01	0.9459			
	Atom1	**Atom2**	$r1$ (bohr)	$r2$ (bohr)	$r1/r2$	$r1-B-r2$ (deg)
	F	Na	2.9088	2.3880	1.2181	180.0000
	F	Mg	2.0687	1.6768	1.2337	180.0000
Na–F	$\rho_b^{max}=0.544829731E-02$	$\nabla^2\rho(r)=0.841E-13$				
Mg–F	$\rho_b^{max}=0.414938856E-01$	$\nabla^2\rho(r)=0.421E-14$				
$NaZnF_3$				52.50%		
Na	1a	+9.2711928354E-01	0.9636			
Zn	1b	+1.4355558499E+00	0.7178			
F	3c	−7.8707395641E-01	0.893			
	Atom1	**Atom2**	$r1$ (bohr)	$r2$ (bohr)	$r1/r2$	$r1-B-r2$ (deg)
	F	Na	2.9875	2.4443	1.2222	180.0000
	F	Zn	1.9041	1.9368	0.9831	180.0000
Na–F	$\rho_b^{max}=0.447950275E-02$	$\nabla^2\rho(r)=0.203E-13$				
Zn–F	$\rho_b^{max}=0.629958050E-01$	$\nabla^2\rho(r)=0.602E-12$				

densityρ_b^{max}; which means that these bonds are very weak with closed shell like characteristic (partially ionic-partially covalent bonds with dominating ionic character).

3.3. Thermal properties

In order to access the properties of solids at relatively low temperatures, the approach commonly employed consists of assuming a harmonic potential for the atoms at any crystal structure: the quasi-harmonic approximation (QHA). At present, the used method is to follow procedure given by Blanco et al. [46]. As a first step, a set of total energy calculation versus primitive cell volume (E–V), in the static approximation, was carried out and fitted with the numerical EOS in order to determine its structural parameters at zero temperature and pressure, and then derive the macroscopic properties as a function of pressure and temperature from the standard thermodynamic relations. The thermal properties are determined in the temperature range from 0.0 to 1000 K where the quasi-harmonic model remains fully valid. The pressure effect is studied in the range from 0.0 to 20 GPa.

The pressure and temperature dependence of the relative volume V/V0 of the $NaMgF_3$ and $NaZnF_3$ is shown in Fig. 8. It is seen that the relative volume V/V0 decreases at the given temperature as the pressure increases. Therefore, the effect of increasing temperature on the $NaZnF_3$ is more apparent. We have examined carefully the behavior of the two most critical magnitudes, thermal expansion coefficient α and Debye temperature Θ, with temperature T are shown in Figs. 9 and 10, respectively. It can be seen that the thermal expansion coefficient increases with T^3 at lower temperatures and gradually approaches to a linear increase at higher temperatures. This latter varies faster for the $NaZnF_3$ compound and has rather a higher value of α. The Debye temperature is also one key quantity in the quasi-harmonic Debye model. In Fig. 9, we show the Debye temperature Θ as a function of temperatures at different pressures of P=0.0, 5.0, 10.0, 15.0 and 20.0 GPa, it is shown that at low pressure, the Debye temperature Θ decreases significantly when the temperature changes from 0.0 to 1000 K.

It can be concluded that the effect of the temperature on the Debye temperature Θ is not as important as that of the pressure on Debye temperature. The higher pressure leads to the low effect on the Debye temperature. Fig. 10 demonstrates that when the temperature is constant, the Debye temperature Θ increases non-linearly with applied pressures, indicating the change of the vibration frequency of particles. The temperature dependent Debye temperature curve in both $NaMgF_3$ and $NaZnF_3$ documents a decreasing trend with enhanced temperature. The outcome is the thermal softening of lattice results from bond expansion and bond weakening due to thermal stress.

The Grüneisen constant γ describes the anharmonicity in the vibrating lattice, and it has been widely used to characterize and extrapolate the thermodynamic behavior of a material at high pressures and temperatures, such as the thermal expansion coefficient and the temperature dependence of phonon frequencies and line-widths. It is also directly related to the equation of state (EOS). The static variation of Grüneisen parameter with temperature T and pressure P is shown in Fig. 11. It can be observed that at given pressure, the γ increases dramatically with the temperature $T>200$ K, while at fixed temperature, the γ decreases dramatically with pressure, and that as the temperature goes higher, the γ decreases more rapidly with the increase of pressure. These results are attributed to the fact that the effect of temperature on the ratio is not as significant as that of pressure, and there will be a large thermal expansion at a low pressure.

4. Conclusions

In this work, we have performed ab initio calculations on the structural, elastic, electronic, and thermodynamic properties for the cubic $NaZnF_3$ and $NaMgF_3$ using the FP-LAPW

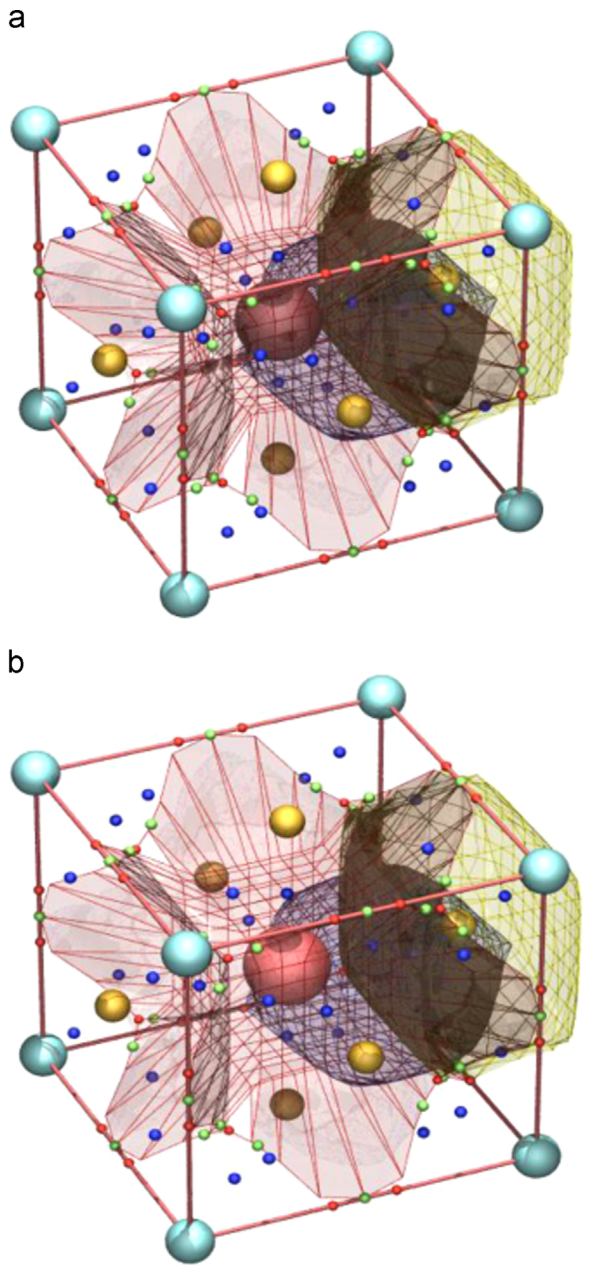

Fig. 7. 3D crystallographic representation of CP's points (balls) and basins for $NaMgF_3$ (a) and $NaZnF_3$ (b). Yellow balls represent the fluorine ions, light blue balls are sodium ions and red balls Zn and Mg ions. Small red balls are placed at Wyckoff's 3c are the $(3,-1)$ bond Cp's and $(3,+3)$ cage Cp's are represented by the small blue balls. (For interpretation of the references to color in this figure legend, the reader is referred to the web version of this article.)

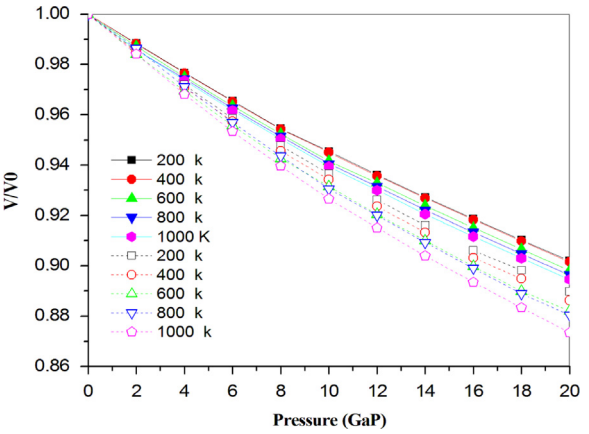

Fig. 8. Pressure and temperature dependence of the relative volume $V/V0$ of $NaMgF_3$ and $NaZnF_3$.

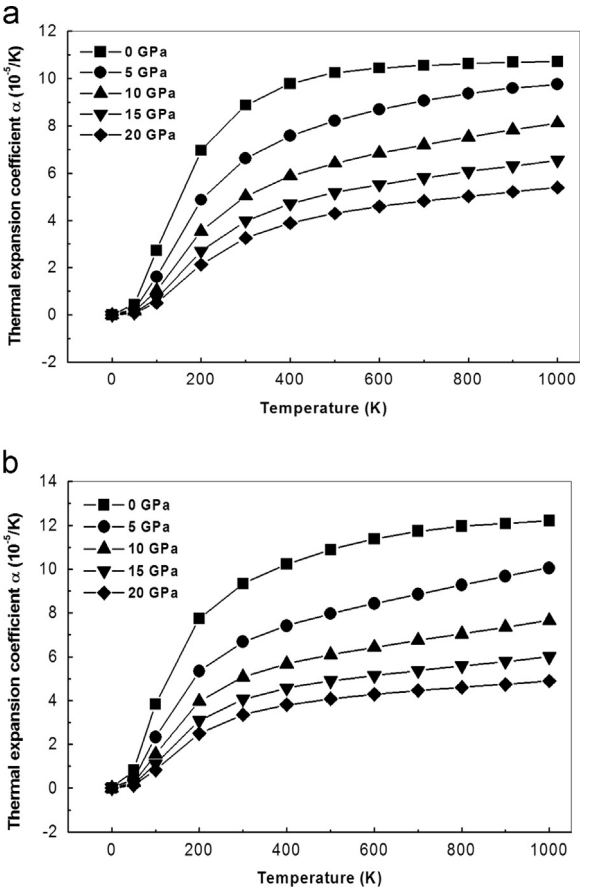

Fig. 9. The thermal expansion α versus temperature at different pressures of $NaMgF_3$ (a) and $NaZnF_3$ (b).

method within PBE-GGA, EV-GGA and mBJ. The most relevant results are summarized as follows: we have determined both $NaZnF_3$ and $NaMgF_3$ are stable in the cubic structure. We succeeded in predicting some elastic properties such as elastic moduli, shear modulus, Young's modulus and Poisson's ratio. As a result, brittleness behavior of these compounds is interpreted via the calculated elastic constants. The calculations of the electronic band structure show an insulating character of these materials with an indirect energy band gap (M–Γ). We note that the mBJ approximation yields larger fundamental band gaps compared to those of PBE-GGA. The analysis of the bonding properties reveals that bonds between the constituting elements of these compounds are mainly ionic. Through the quasi-harmonic Debye model, the dependences of the volume,

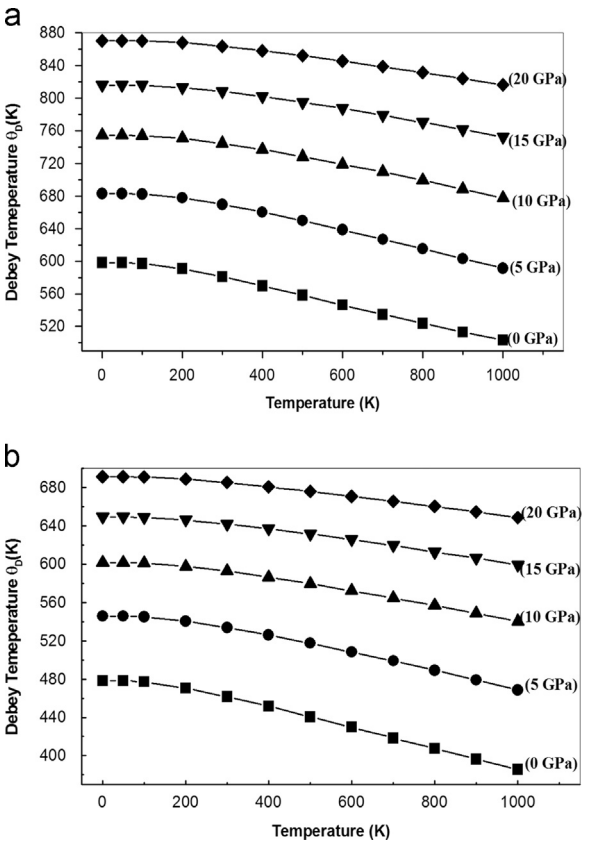

Fig. 10. The variation of the Debye temperature θ_D versus temperature at different pressures of $NaMgF_3$ (a) and $NaZnF_3$ (b).

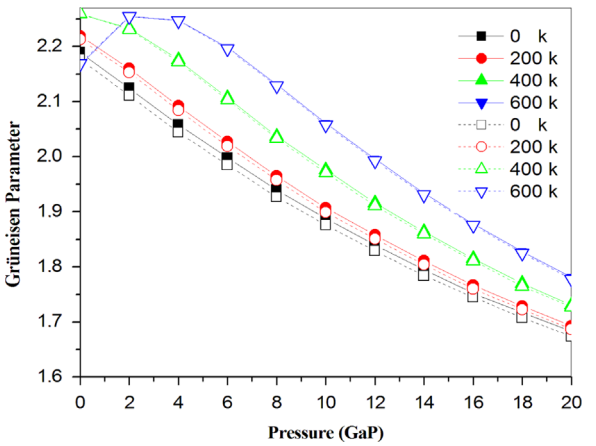

Fig. 11. Static variation of the Grüneisen parameter with temperature T and pressure P.

bulk modulus, and Debye temperature on temperature and pressure have been obtained successfully.

Acknowledgments

Authors (K. R, A. B and S.B.O) acknowledge the financial support by the Deanship of Scientific Research at King Saud University for funding the work through the research group Project no. RPG-VPP-088.

References

[1] R. Terki, H. Feraoun, G. Bertrand, H. Aourag, Phys. Status Solidi B 242 (2005) 1054.
[2] C.E. Runge, A. Kubo, B. Kiefer, Y. Meng, V.B. Prakapenka, G. Shen, R.J. Cava, T.S. Duffy, Phys. Chem. Miner. 33 (2006) 699.
[3] S. Cabuk, H. Akkus, A.M. Mamedov, Physica B 394 (2007) 81.
[4] H. Wang, B. Wang, R. Wang, Q. Li, Physica B 390 (2007) 96.
[5] G. Horsch, H. Paus, J. Opt. Commun. 60 (1986) 69.
[6] S. Sugano, R.G. Shulman, Phys. Rev. 130 (1963) 517.
[7] B. Kleinman, M. Karplus, Phys. Rev. B 3 (1971) 24.
[8] T.F. Soules, J.W. Richardson, D.M. Vaught, Phys. Rev. B 3 (1971) 2186.
[9] K. Umemoto, R.M. Wentzcovitch, Phys. Rev. B 74 (2006) 224105.
[10] T.F. Soules, E.J. Kelly, D.M. Vaught, J.W. Richardson, Phys. Rev. B 6 (1972) 1519.
[11] R.G. Shulman, Y. Yafet, P. Eisenberger, W.E. Blumberg, Proc. Nat. Acad. Sci. U. S. A 73 (1976) 1384.
[12] T. Ouahrani, I. Merad-Boudia, H. Baltache, R. Khenata, Z. Bentalha, Phys. Scr. 84 (2011) 025704.
[13] G. Vaitheeswaran, V. Kanchana, R.S. Kumar, A.L. Cornelius, M.F. Nicol, A. Svane, A. Delin, B. Johansson, Phys. Rev. B 76 (2007) 014107.
[14] K. Umemoto, R.M. Wentzcovitch, D.J. Weidner, J.B. Parise, Geophys. Res. Lett. 33 (2006) L15304.
[15] Y. Zhao, D.J. Weidner, J.B. Parise, D.E. Cox, Phys. Earth Planet. Inter. 76 (1993) 17–34.
[16] J. Chen, H. Liu, C.D. Martin, J.B. Parise, D.J. Weidner, Am. Mineral. 90 (2005) 1534.
[17] G.A. Geguzina, V.P. Sakhnenko, Cryst. Rep. 49 (2004) 15.
[18] E. Sjöstedt, L. Nordstrom, D.J. Singh, Solid State Commun. 114 (2000) 15.
[19] P. Hohenberg, W. Kohn, Phys. Rev. B 136 (1964) 864.
[20] W. Kohn, L.J. Sham, Phys. Rev. A 140 (1965) 1133.
[21] P. Blaha, K. Schwarz, G.K.H. Madsen, D. Kvasnicka, J. Luitz, Technisch Universitat, Wien, Austria, ISBN 3-9501031-1-2, 2001.
[22] J.P. Perdew, K. Burke, M. Ernzerhof, Phys. Rev. Lett. 77 (1996) 3865.
[23] E. Engel, S.H. Vosko, Phys. Rev. B 47 (1993) 13164.
[24] F. Tran, P. Blaha, Phys. Rev. Lett. 102 (2009) 226401.
[25] P.E. Blochl, O. Jepsen, O.K. Anderson, Phys. Rev. B 49 (1994) 16223.
[26] T. Ouahrani, J.M. Menendez, M. Marque´s, J. Contreras-Garcı´a V.G. Baonza, J.M. Recio, EPL 98 (2012) 56002.
[27] S. Yakovlev, M. Avdeev, M. Mezouar, J. Solid State Chem. 182 (2009) 1545.
[28] A. Reuss, A. Angew, Mater. Phys. 9 (1929) 49.
[29] W. Voigt, Teubner, Leipzig, 1928.
[30] M.J. Mehl, B.M. Barry, D.A. Papaconstantopoulos, in: J.H. Westbrook, R.L. Fleis cheir (Eds.), Intermetallic Compounds: Principle and Practice, Vol. I, Principles Wiley, London, 1995, pp. 195–210. (Chapter 9).
[31] Z. Hashin, S. Shtrikman, J. Mech. Phys. Solids 10 (1962) 335.
[32] J. Haines, J.M. Leger, G. Bocquillon, Annu. Rev. Mater. Res. 31 (2001) 1.
[33] S.F. Pugh, Philos. Mag. 45 (1954) 823.
[34] I.N. Frantsevich, F.F. Voronov, S.A. Bokuta, in: I.N. Frantsevich (Ed.), Handbook, Naukuva Dumka, Kiev, 1983, pp. 60–180.
[35] G. Vaitheeswaran, V. Kanchana, R.S. Kumar, A.L. Cornelius, M.F. Nicol, A. Svane, A. Delin, B. Johansson, Phys. Rev. B 76 (2007) 014107.
[36] T. Seddik, R. Khenata, O. Merabiha, A. Bouhemadou, S. Bin-Omran, D. Rached, Appl. Phys. A 106 (2012) 645.
[37] P. Mori-Sánchez, A.J. Cohen, Y.W. Yang, Phys. Rev. Lett. 100 (2008) 146401.
[38] R.G. Parr, R.G. Pearson, J. Am. Chem. Soc. 105 (1983) 7512.
[39] A. Otero-de-la-Roza, M.A. Blanco, A. Martin Pendás, V. Luaña, Comput. Phys. Commun. 180 (2009) 157.
[40] R.F.W. Bader, Phys. Rev. B 49 (1994) 13348.
[41] P. Mori-Sánchez, A. Martin Pendás, V. Luaña, J. Am. Chem. Soc. 124 (2002) 14721.
[42] V. Luaña, A. Costales, A.M. Pendás, L. Pueyo, J. Phys.: Condens. Matter 11 (1999) 6329.
[43] R.F.W. Bader, T.S. Lee, D. Cremer, E. Kraka, J. Am. Chem. Soc. 105 (1983) 5061.
[44] V. Luaña, A. Costales, A.M. Pendás, Phys. Rev. B 55 (1997) 4285.
[45] T. Ouahrani, A. Otero-de-la-Roza, A.H. Reshak, R. Khenata, H.I. Faraoun, B. Amrani, M. Mebrouki, V. Luaña, Physica B 405 (2010) 3658.
[46] M.A. Blanco, E. Francisco, V. Luaña, Comput. Phys. Commun. 158 (2004) 57.